Hindawi
Shock and Vibration
Volume 2022, Article ID 1609981, 15 pages
https://doi.org/10.1155/2022/1609981

Research Article

Comprehensive Structural Assessment of a Perforated Plate in the Edge and Central Crack

Nooredin Sabzian Morad Abadi,[1] Mojtaba Nazari ,[1] and Hamed Bazvandi[2]

[1]*Department of Mathematics, Khorramabad Branch, Islamic Azad University, Khorram Abad, Iran*
[2]*Department of Mechanical Engineering, Khorramabad Branch, Islamic Azad University, Khorram Abad, Iran*

Correspondence should be addressed to Mojtaba Nazari; mojtabanazari_1350@yahoo.com

Received 21 June 2022; Revised 5 July 2022; Accepted 6 July 2022; Published 3 August 2022

Academic Editor: S. Mahdi S. Kolbadi

Injury domain method does not let the cracks close to the critical level to start growing and lead to the critical length before the time of periodic visits. Until now, calculation method of the tension in a perforated plate has been assessed in two- or three-dimensional mode by considering the special opening (holes with different geometry). But, the tension calculation in a plate included opening with edge crack presence in three-dimensional mode has not been studied. So, in this study, in addition to the assessment of this mode, calculation method of the tension in the plates including different opening will be assessed. Generally, when the object endures the tensions for a long time, the geometric deformation will be occurred. Used plates in this study are made of isotropic materials. In these materials, when the force is applied, they show the same function in any direction and the direction of applying force has any on effect their treatment. For analyzing the data, the Abaqus software is used. The results of the research show that the kind of the boundary conditions has effect on the value of critical load in the tension and kind of created tension. In the joint-joint boundary conditions, tension critical load increases with length-to-width ratio increase, and local tension occurred in the higher penetration ratio. However, in the joint-open boundary conditions, by increasing the length-to-width ratio, the tension critical load is decreased and in often cases, the tensions are kind of general. According to this, the plates including cavity with bigger dimensions are subjected to local tension in smaller ratios of yielding dimension.

1. Introduction

Effect of boundary conditions on tension loading of perforated plate included yielding, the boundary conditions is one of the most important parameters in the value of critical load. In many of structures and mechanical parts, the germination and crack growth is an inevitable phenomenon, for example, in welded parts like, metal structures in the big airplanes, sea structures, bridges, under pressure reservoirs, and also in forging productions like, turbine rotors and generators in the powerhouses [1–3]. Under the intermittent loading, the injuries caused by fatigue are the main factor in the failure of industrial parts [4]. The crack existence in the mechanical components causes decrease in the value of load ability and fatigue life and makes them weaken [5]. Identification and having a correct understanding of this phenomenon can prevent or decrease its breakdowns [6]. There are several methods to control the crack growth under static or fatigue loading and the crack growth can be restrained by replacement of injured parts, decreasing of possible loads, or decreasing of crack growth rate to acceptable level [7]. Replacement of the injured parts is usually costly [8]. Also decreasing of possible loads is sometimes impermissible and can have effect on the correct function of parts [9]. Decreasing the crack growth rate and receiving it to an acceptable level is an economic method faced with fatigue cracks, which decreases the costs and has no lateral effects on the other components [10]. In addition to this, the philosophy of advanced components designing is different than usual methods for designing of structures. The usual methods are based on principles of material strength, it means, how much a material or a structure has strength against the injury. The new concepts are based on the injury domain principle near the strength principles, it means, after

the injury creation, the injured material should have the ability to continue its working [11–13].

This method helps the user to decrease the repair costs and replacement of injured parts and also decrease the probability of failure and fatigue of parts in the service time. The design based on strength principles depends on the allowable design values, generally, these values are taken from specific experiments and are corrected by confidence coefficients. The confidence coefficients are considered for the proximity of values difference among the considered limitations in designing (the changes in material properties, the environmental conditions, loading in the combined conditions, etc.,) and real conditions of the components during the service [14–16]. Usually, when the fatigue loading is considered, the permissible coefficients of designing are got from static loading and also the confidence coefficients have higher values [17]. On the other hand, a different kind of the opening and notches are created in different sizes and shapes in the engineering structures, because of different reasons like: decrease of structures weight, ability of equipment connection to them, and output and input paths creation. This opening causes creation of intense local tensions which is named tension concentration. The tension concentration is effective in the decrease of useful life and the confidence coefficient of structure around these discontinuities (opening and cracks). On the other hand, determination of the tension value and the points of tension concentration in the experimental methods are usually costly and difficult [18].

One of the main problems of the crack growth analysis is by using finite element methods, in which, the structure reticulation should be changed frequently until the analysis is done with suitable accuracy, but this is a heavy and time-consuming analysis. If the analytical answers are found, their results can be simulated easily through available software so that the frequent experimental tests that cost heavy and are time-consuming can be removed [19]. By increasing or decreasing the tensions or, in other words, the changes in the applying force, the object will be fatigued. The determination of fatigue life can prevent the financial losses and irreparable damages [20]. Also, because the structure load-bearing capacity depends on the value of tension concentration severely, and the value of material fatigue life in designing of the structures, paying attention to the tension concentration issue and material fatigue life and also the plate defects like crack existence in the plates including opening with different shapes is an inevitable matter which some researchers have studied about for several years [21]. The crack existence in objects is one of the most important problems in the industry, and finding the methods to forecast of crack growth and solving it has a specific importance. So, the parameters like the fatigue, buckling, and object yield should be considered in the designing.

2. Research Background

In a research, Hasebe and teammates explained the relations related to the problem solving of two-dimensional thermoelastic for the plate including opening completely. In this study, they used mixed variable method to present their relations. The mixed potential functions were extracted for the used mapping functions in this study, and also for different boundary conditions and temperature conditions [22]. Aseeri used mixed variable method to get the potential functions for an unlimited elastic plate including opening with different shapes. For accessing a straight method, this opening was written to out of a circle with single radius, by using suitable and concerted mapping function [23]. Vinh et al. evaluated the confrontation between cracked opening and its progress under uniform thermal flow. Their results showed that the confrontation between cracked opening and leaner crack of uniform thermal flow leads to elimination of tension intensity coefficients in the tip of the edge crack [24]. Gao and teammates presented an accurate solution for the tension analysis of piezoelectric plate including the crack or oval opening. Recently, by using of mixed variable method and integral equations solution and by using of Cauchy integral and fractional mapping functions, different openings in the unlimited isotropic plates were studied [25].

Xu and teammates, in 2010, did a three-dimensional thermoelastic analysis on a rectangular plate with a length, b width, and h thickness in which the above surface was flat and the down surface was defined with a continuous function and was exposed to stable mode temperature and mechanical load [26]. Sarkar and Lahiri, in 2012, assessed a three-dimensional issue in a semi-infinite, homogeneous, isotropic, and thermoelastic space with a thermal source depended on the time was located on its border. In this study, they used normal analysis and eigenvalue method to solve the unpaired equations [27]. In 2013, Hou and teammates got the three-dimensional solution of governing equations in the stable mode for the isotropic materials. They assumed two displacement functions for simplification of the governing equations, then by using differential operator theory, they expressed three general methods in two functions and solved the issue by using two different kinds of thermal loading. In the first issue, a spot thermal source into the infinite thermoelastic object, and in the second one, a thermal source on a thermoelastic semi-infinite surface were considered [28].

3. Method

3.1. Tension Models. Structural assessment of a homogeneous and rounded plate based on analytical solution and numerical solution and comparing the tension modes results are represent in Figure 1. Also, the homogeneous plate and its loading kind are shown, and the material properties and its boundary conditions are expressed in Tables 1 and 2:

$$N_{X,CR} = \pi^2 a^2 D \frac{1}{m^2} \left(\frac{m^2}{a^2} + \frac{n^2}{b^2} \right)^2. \quad (1)$$

Value of the critical force per unit length [20] is as follows:

n: half wave number in line with y

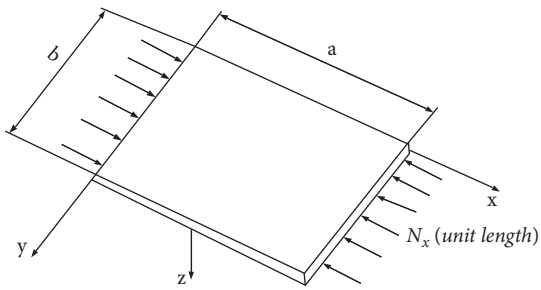

Figure 1: Flat plate under the pressure loading and included joint boundary conditions [29].

Table 1: Sample properties.

Index	Properties	Value
a	Plate length	20 in
b	Plate width	10 in
h	Plate thickness	0.1 in
E	Young module	10e6psi
Nu	Poisson's coefficient	0.3
D	Hardness	916 lb-in

Table 2: Presented boundary conditions.

$x = 0,\ a$	$w = 0$	$M_x = 0$
$y = 0,\ b$	$w = 0$	$M_y = 0$

m: half wave number in line with x

The minimum critical force in this mode is equal to 1 ($n = 1$) [20]:

$$N_{X,CR} = \Pi^2 a^2 D \frac{1}{m^2}\left(\frac{m^2}{a^2} + \frac{1^2}{b^2}\right)^2 N_{X,CR} = \frac{k\pi^2 D}{b^2}. \quad (2)$$

The critical force relation [22] is

$$\sigma_{CR} = \frac{k\pi^2 E}{12\left(1 - \nu^2\right)}\left(\frac{t}{b}\right)^2. \quad (3)$$

The tension coefficient relation (k) with a/b ratio and tension modes (m) can be extracted here [22]:

$$k = \left(\frac{mb}{a} + \frac{a}{mb}\right)^2. \quad (4)$$

Relation of tension modes change [21] is as follows:

$$\frac{mb}{a} + \frac{a}{mb} = \frac{(m+1)b}{a} + \frac{a}{(m+1)b}\frac{a}{b} = \sqrt{m(m+1)}. \quad (5)$$

According to the obtained values of the tension coefficient (Figure 2 and Table 3), the least value of tension critical load is seen in the second mode ($m = 2$). In this situation, there is a sinusoidal half wave in the transverse direction and there are two half waves in the longitudinal direction. In this mode ($m = 2$), the value of critical force is obtained through analytical solution and by software as in Tables 4–6.

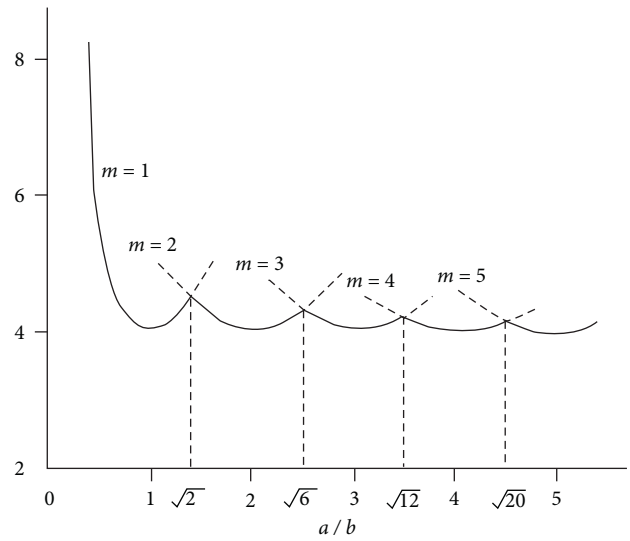

Figure 2: Tension coefficient figure (k) based on a/b ratio for different values of m (modes transformation) for the joint plate [22].

Table 3: Values of k based on tension modes.

$m = 1$	$K = 6.25$
$m = 2$	$K = 4$
$m = 3$	$K = 4.694444$
$m = 4$	$K = 6.25$
$m = 5$	$K = 8.41$
$m = 6$	$K = 11.11111$
$m = 7$	$K = 14.33163$

Table 4: Value of critical force obtained through analytical solution and solution by software.

Analytical solution	Pcr-tahlili = 3616.223
Solution by software (the shell element)	Pcr-shell = 3613.2
Solution by software (the solid element)	Pcr-solid = 3596.7

Table 5: Percentage difference of analytical solution and software solution for the least tension mode.

Relation	Percentage difference
((Pcr-tahlili – Pcr-shell)/Pcr-tahlili) ∗ 100	0.08% shell
((Pcr-tahlili – Pcr-solid)/Pcr-tahlili) ∗ 100	0.5% solid

Table 6: Percentage difference of software solution and analytical solution for other tension mode kinds.

Tension mode	Analytical solution	Software solution	Percentage difference (%)
$m = 1$	5650.349	5646.0	0.07
$m = 2$	3616.223	3613.2	0.08
$m = 3$	4244.04	4239.0	0.11
$m = 4$	5650.349	5641.4	0.15
$m = 5$	7603.109	7586.0	0.22
$m = 6$	10045.06	10015	0.29
$m = 7$	12956.6	12908	0.37

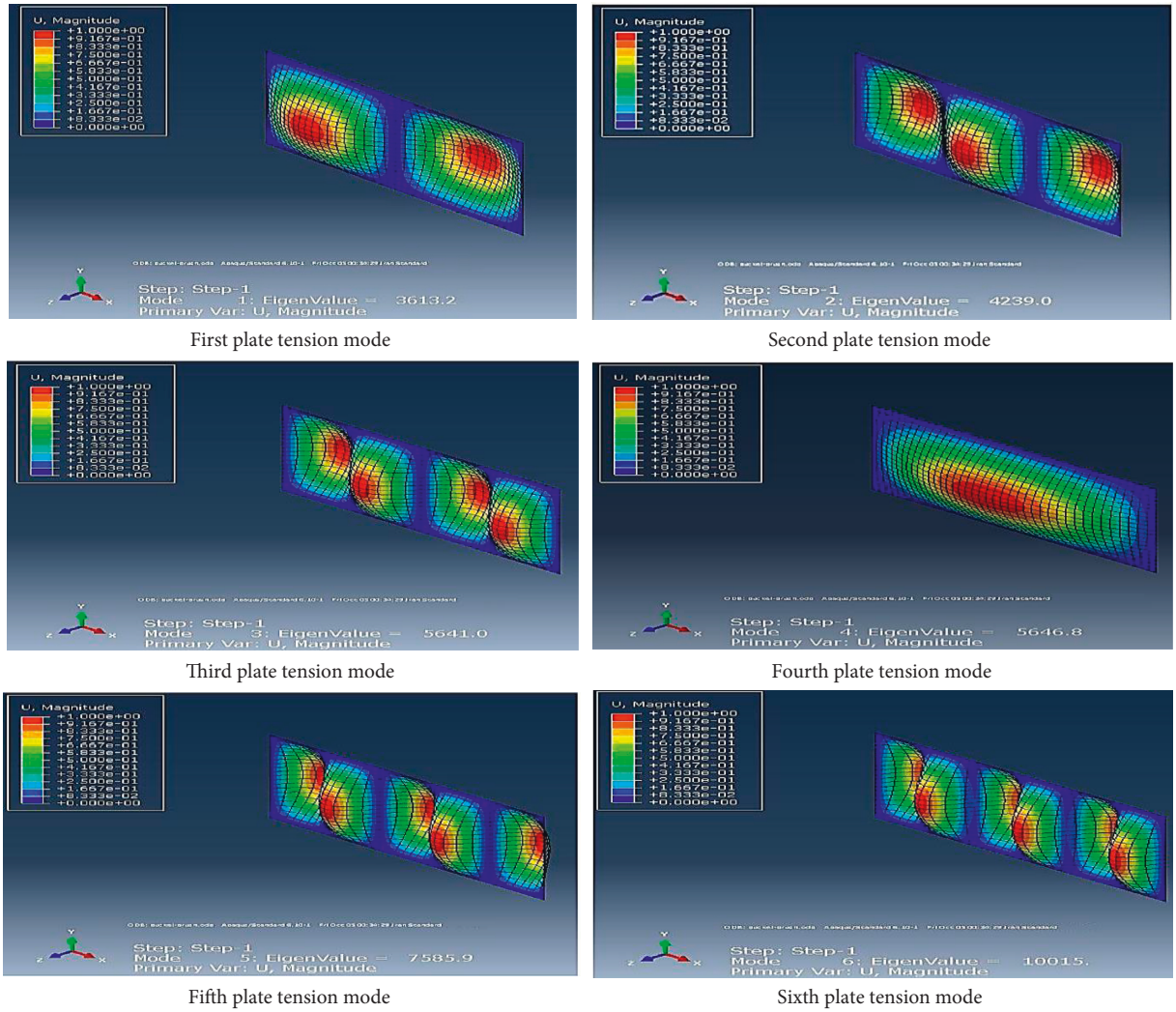

First plate tension mode

Second plate tension mode

Third plate tension mode

Fourth plate tension mode

Fifth plate tension mode

Sixth plate tension mode

Figure 3: Tension modes of homogeneous and isotropic plate.

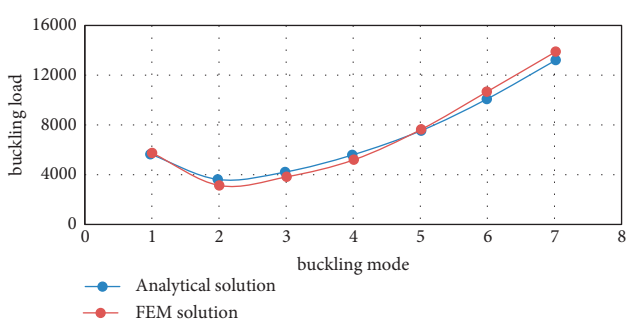

Figure 4: Comparison of the tension values from the software and analytical solution.

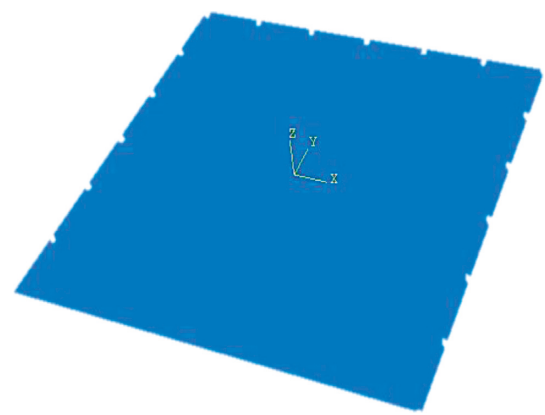

Figure 5: Plate loading and applied support conditions.

The treatment figure of tension modes shows that the least of tension value in this sample occurred in mode 2. And it shows that the mode 2 is sensitive for this kind of boundary and loading conditions (Figure 3). By increasing the modes, the values of tensions have uptrend, and in this value, the first mode shape, is the fourth created tension mode in the plate. Due to the high accuracy and proximity of obtained results from finite element analysis and analytical solution, both the obtained figures with matched each other (Figure 4).

In this model, the effects of circular cavity dimensions in a plate on the critical value of tension load were evaluated. The plate dimensions are 120 mm × 120 mm

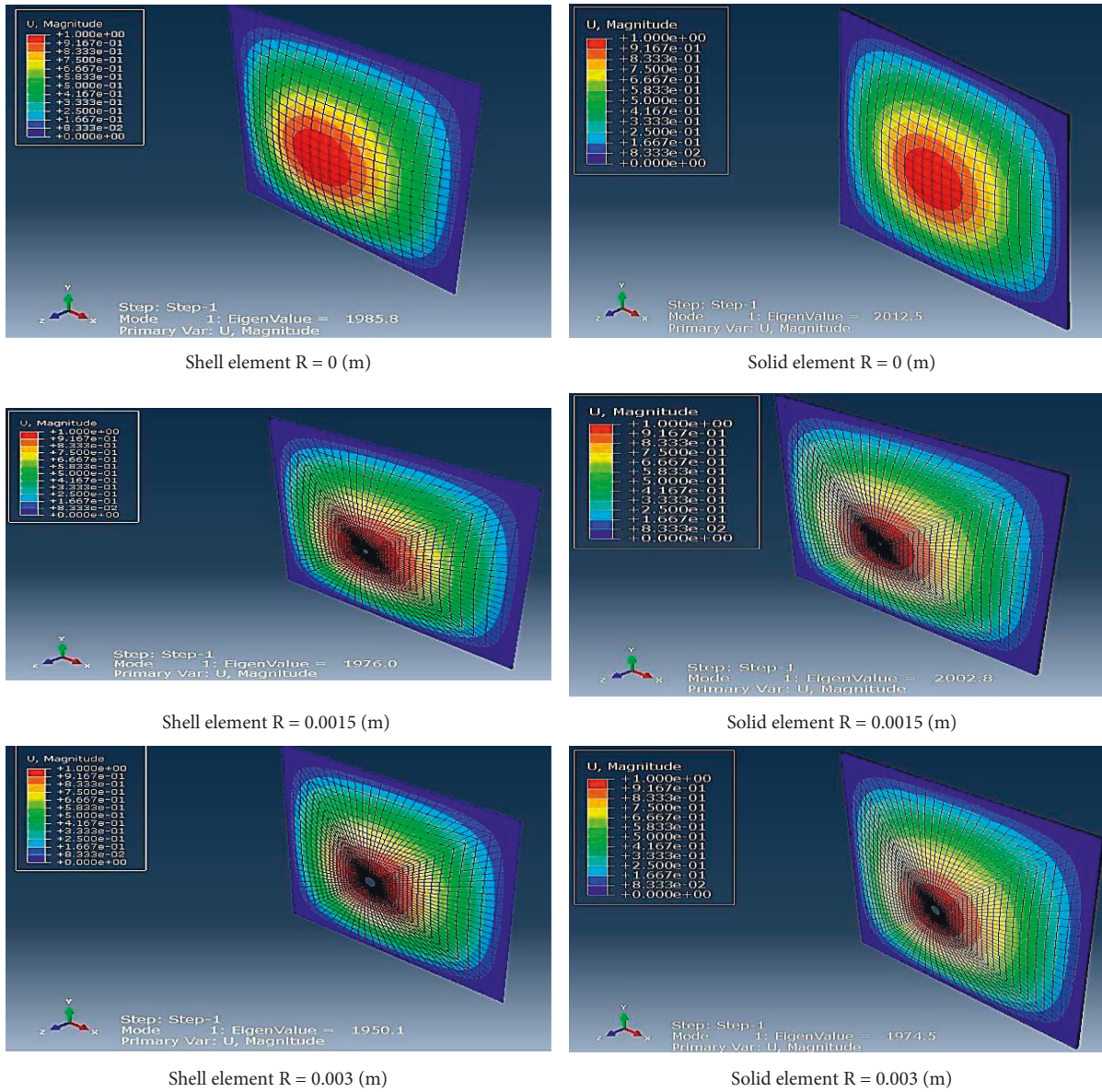

Shell element R = 0 (m) Solid element R = 0 (m)

Shell element R = 0.0015 (m) Solid element R = 0.0015 (m)

Shell element R = 0.003 (m) Solid element R = 0.003 (m)

Figure 6: Plate tension with different cavity radii.

Table 7: Specifications of presented sample.

Index	Properties	Value
A	Plate length	0.12 m
B	Plate width	0.12 m
H	Plate thickness	0.0012 m
$E1$	Young module in line with fibers	130 GPa
$E2$	Young module in the transverse direction	10 GPa
$E3$	Young module out of plate	10 GPa
$G12 = G13$	Torsional modulus	5 GPa
Nu12 = Nu13	Poisson's coefficient	0.35
Nu23 = Nu32	Poisson's coefficient	0.49

(length and width) (Figures 5 and 6). Each of the four edges are closed by the joint support in line with $\underline{z}$ and perpendicular to the plate, and a pressure load in line with $\underline{x}$ was applied in both opposite edges such that the $\underline{x}$ axis is perpendicular to them. For the plate stability, we close one of the loaded edges in line with $\underline{x}$ and also, we close the middle point of this edge in line with $\underline{y}$ (Tables 7–9 and Figure 7).

Table 8: Introduction of used parameters in the modeling.

R (m)	Cavity radius
d/b	Ratio of cavity diameter to plate width
N_x (N/m)	Critical load value to length unit
$K_c = (N_x * b)/(E_2 * h^3)$	Value of dimensionless tension load by shell software
$K_c = (N_x * b)/(E_2 * h^3)$	Value of dimensionless tension load by solid software
Kc article	Value of dimensionless tension load of article

Table 9: Comparing dimensionless values of critical tension load for shell and solid elements.

R (m)	d/b	N_x (n/m)	Kc shell	Kc solid	Kc article
0	0	1985.0	13.79	13.97	13.79
0.0015	0.025	1976.00	13.72	13.93	13.71
0.003	0.05	1950.00	13.54	13.71	13.51
0.006 m	0.1	1859.70	12.90	13.07	12.80
0.012	0.2	1615.00	11.21	11.30	10.82
0.018	0.3	1393	9.67	9.75	8.97
0.024	0.4	1226.4	8.51	8.53	7.51
0.03	0.5	1106	7.67	7.73	6.39
0.036	0.6	1011.7	7.02	7.04	5.63
0.042	0.7	900	6.25	6.31	4.99
0.048	0.8	719	4.99	5.08	4.43

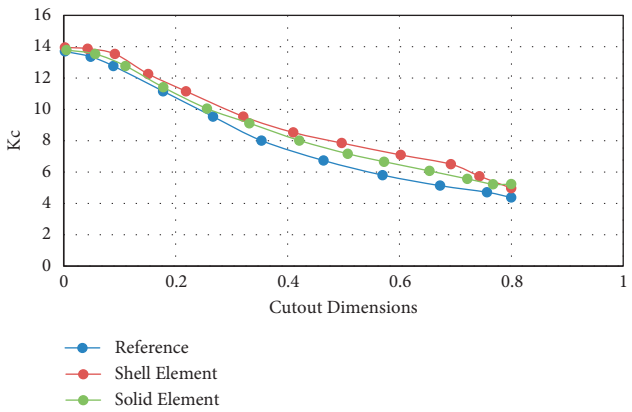

Figure 7: Results from shell and solid elements.

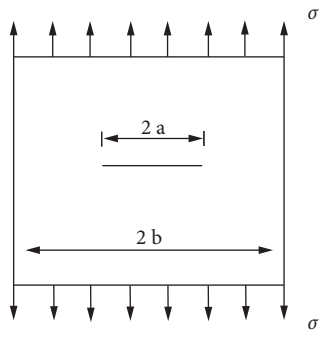

Figure 8: Plate with limited width including central crack [23].

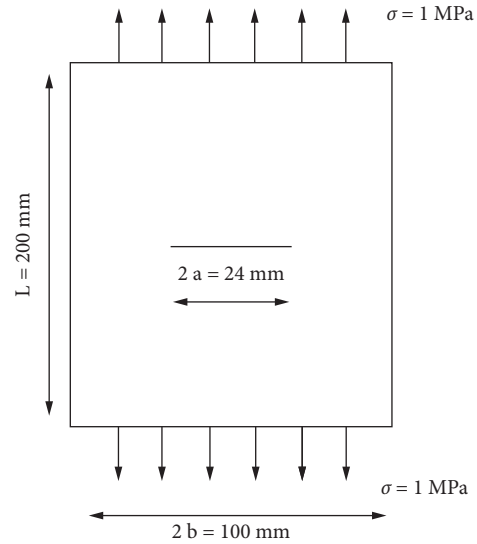

Figure 9: Plate with central crack under uniform tension [23].

3.2. Crack Modeling. This factor for the plate with big width and a central gap and 2a length is showed in Figure 8. In the event that the plate width be limited and equal to 2b, the correction coefficient should be considered $f(g)$ to enter the tension effect of crack tip in the tension intensity factor. In this mode, the tension intensity factor is equal to

$$k_i = \sigma\sqrt{\pi a}\left(\frac{2b}{\pi a}\tan\left(\frac{\pi a}{2b}\right)\right)^{1/2}. \quad (6)$$

In Figure 9 an aluminum plate ($E = 72.4 \times 10^3$ MPa, $\nu = 0.3$) with 200 mm length, 100 mm width, and 1 mm thickness, including a central crack with 24 mm length, under the uniform tensile load equal to 1 MPa is showed. Calculation of tension intensity factor through finite element method and its comparison with analytical method is assessed.

Since the issue geometry is symmetrical, in order to have easiness in the modeling, and also to decrease the time of issue solution, just above a quarter and the right part was modeled (Figure 10).

The S8R element was used and the meshing was done as shown in Figure 11.

The results from the software and the values from the theory relation are shown in Table 10.

As the second sample, for the finite element modeling, the plate with two edge cracks is used. The plate geometry is under uniform tension with two edge cracks which is created perpendicular to direction of entered load and is shown in Figure 12. In this mode, the results obtained from the software analysis is compared with the numerical method which is presented in source [29].

A thin square plate with 10 m length under the flat tension including two edge cracks each 2 m in length are pulled in remote with 10 MPa tension constantly. As mentioned, for this model, the source [30] was used by using numerical solution based on energy method in analyzing the presented crack (the J Integral method). In this source, the

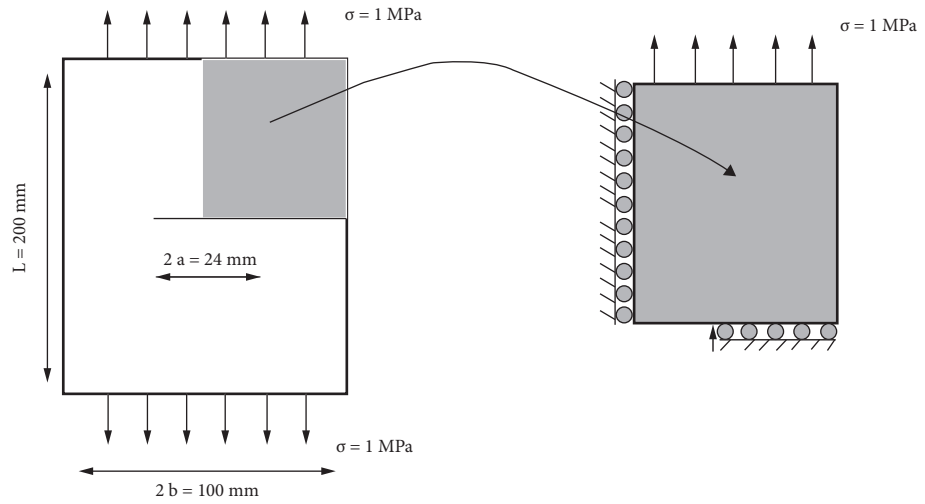

Figure 10: Using symmetry in finite element modeling of first simple issue [24].

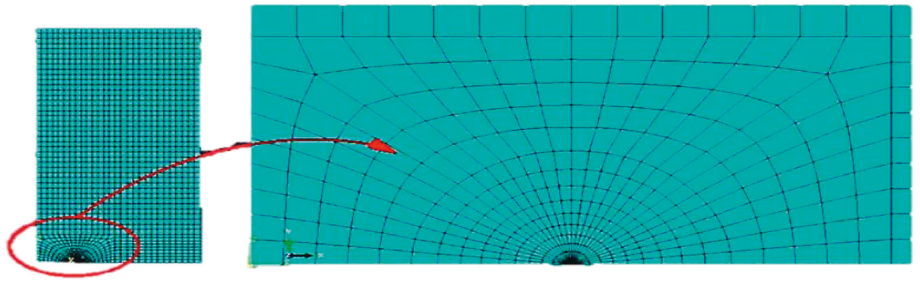

Figure 11: Meshing of the first sample model.

Table 10: Comparing the results for plate including central crack.

Error rate (%)	Finite element method answer	Analytical answer
1.13	$K_I = 6.363$ MPa $(\text{mm})^{0.5}$	$K_I = 6.292$ MPa $(\text{mm})^{0.5}$

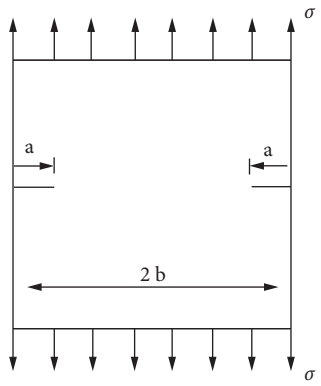

Figure 12: Plate with two edge cracks under tension [25].

values obtained from tension intensity factor, with numerical method used for the third cantor, are the closest values to accurate solution (7% error) and are more than the real values. Table 11 shows the obtained results from finite element solution through Abaqus software compared with the source [31] numerical results. According to this, in mentioned source, used accuracy in the Abaqus software is more than the numerical solution. The assumptions raised regarding this model and the behavioral model as well as the boundary conditions, and it is necessary to point out that the change in each of these cases, including the density and dimensions of the mesh, may cause changes, albeit limited, in the new responses given in the numerical analysis methods.

3.3. 3D Modeling of Edge Crack. In the modeling done, an edge crack is defined in the object, and due to the different thicknesses of object, the values of K_I were calculated along the crack length. For the modeling, the 25 knots brick element was used and the value of applied tensile tension is 50 Mpa. In Table 12, the specifications of modeling sample are presented. Also, in Figure 13, kind of loading and the situation of crack in the object are showed.

One of the most important points in the crack modeling is the singularity of elements in the tip of the crack. This matter is defined by using higher order elements and also transferring the middle knots of the elements in the tip of the crack to 1/4 distance from the tip of the crack. In Figures 13 and 14, a 20 knots element including singularity is shown.

Table 11: Comparing results for the plate including edge crack.

Error rate (%)	Numerical answer of source	Answer of finite element method	Analytical solution
0.8	$K_I = 32.18$ MPa $(\text{mm})^{0.5}$	$K_I = 28.98$ MPa $(\text{mm})^{0.5}$	$K_I = 29.23$ MPa $(\text{mm})^{0.5}$

Table 12: Geometry specifications of three-dimensional object including edge crack.

$A = 2$ w 40 mm	Plate length
$B =$ w 20 mm	Plate width
$a = 0.5$ w 10 mm	Crack length
$t = 2$, 10 and 20 mm	Plate thickness
σ = 50MPa	Tensile tension

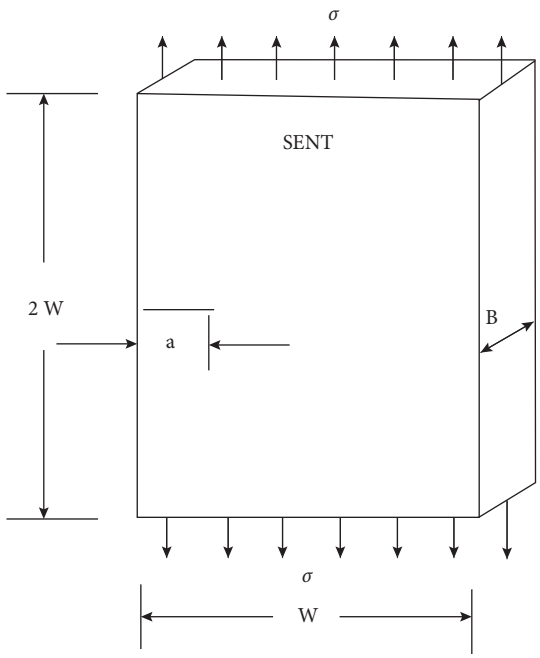

Figure 13: Loading kind and the situation of crack in three-dimensional object [26].

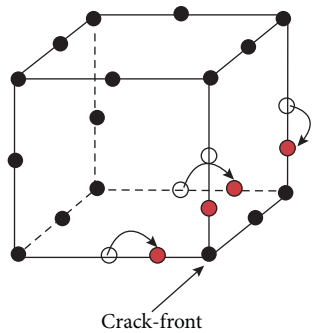

Figure 14: Transferring middle knots of elements in tip of crack to 1/4 distance [26].

The mesh properties such as number and pattern have great effects on analysis results. In the crack modeling, due to the importance of elements' shape in the tip of the crack and its surrounding area, the correct meshing will have double importance. In Figure 15, the meshing method in source [32] is shown.

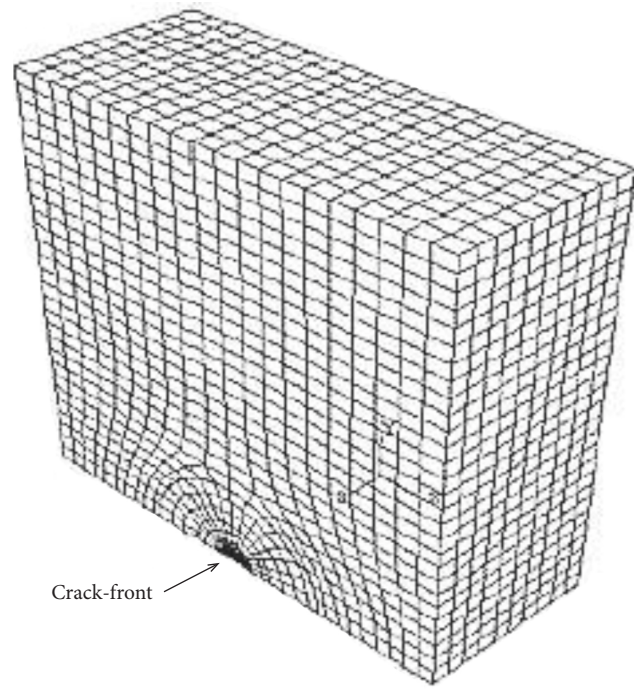

Figure 15: Kind of meshing done [32].

The modeling done for each thickness and their meshing is shown in Figure 16. Figure 17 shows the kind of crack opening under the tensile loading, and also shows the elements and the meshing around of the tip of the crack for the sample with 20 mm thickness.

3.4. Results Comparison. In Figures 18 and 19, the different thicknesses of object are modeled with crack length to 0/5 plate width ratio. The changing process of fatigue values shows that the maximum value of tension intensity is in center of object. Also, by increasing the sample thickness, the maximum value of tension intensity is decreased, but a wider domain of the object is surrounded this value. By comparing the source results with obtained results through finite element solution and 0/2% error, the corrected values of obtained results are obtained.

4. Analysis

In the main presented sample, effects of the yielding dimensions on the tension loading were assessed [34]. One of the factors in the yielding creation in the plate is drilling operation. The drilling causes the injuries like yielding, sharp bulge in plates, visible prominences and fibers shaving and protrusion [35]. In fact, the small splinters are a kind of pollution and wrinkles, around the

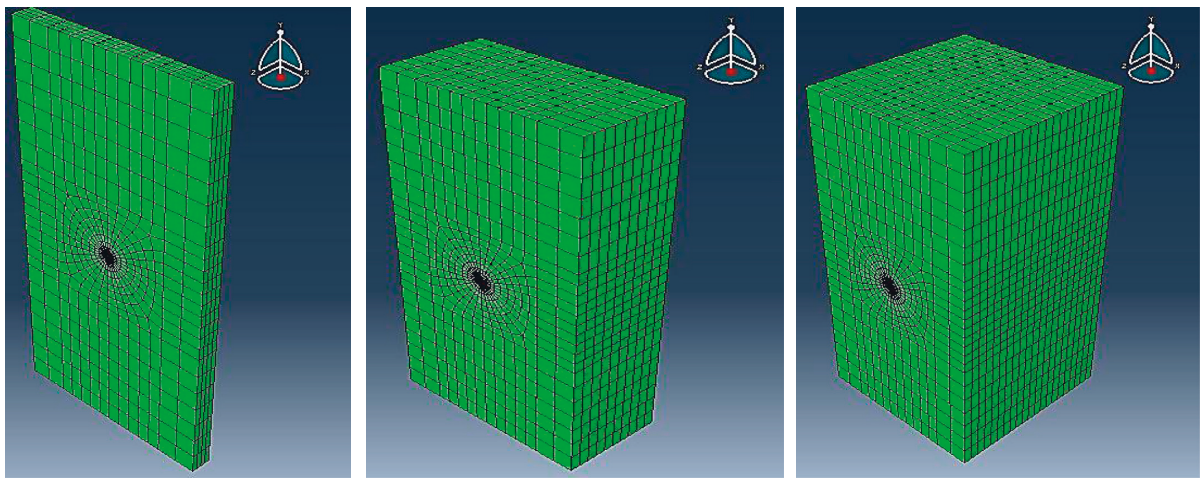

Figure 16: Meshing and modeling of object with different thickness.

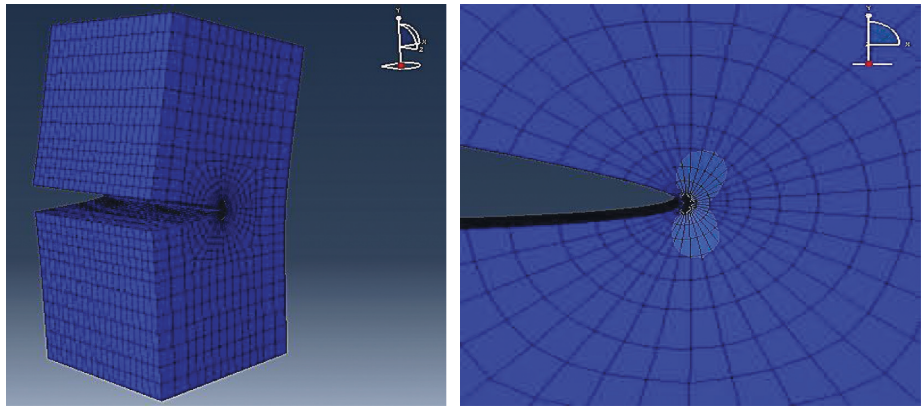

Figure 17: Meshing around the tip of crack and kind of opening of the object under tensile load.

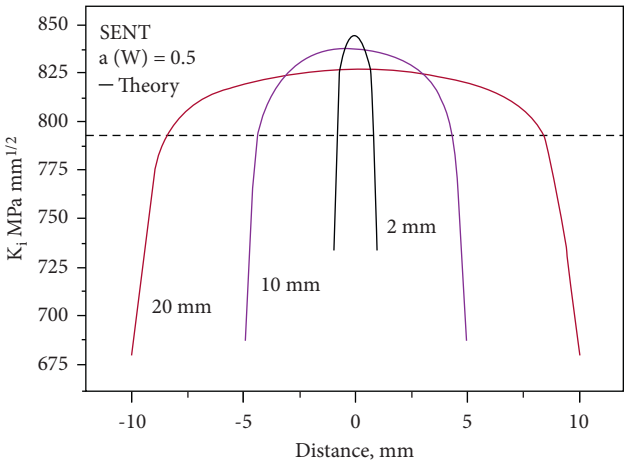

Figure 18: Values of tension intensity for different thicknesses based on source [33].

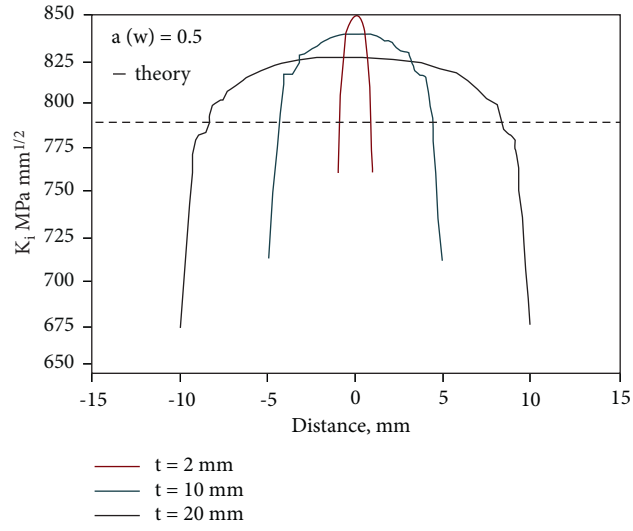

Figure 19: Values of tension intensity for different thicknesses based on finite element method [33].

cavity. Also, thermal injuries and comprehensive yielding are kind of injuries caused by drilling. The yielding is considered as an injury in the drilling plate, and because of it, this phenomenon is analyzed and assessed separately in the plate. The yielding phenomenon also can be created in the down bruise strength and it decreases the material strength in the loading, less than material fatigue and can decrease the operating life of the part.

Table 13: Comparing obtained results from 1/4 modeling and complete modeling.

Sample dimensions	Complete sample joint-free	1/4 sample joint-free boundary conditions	Percentage difference	Complete sample joint-joint	1/4 sample joint-joint boundary conditions	Percentage difference
$b/w = 1$	87.578	87.484	0.107333	151.75	145.69	3.99341
$b/w = 1.5$	36.288	36.575	0.784689	144.80	140.18	3.190608
$b/w = 2$	23.584	23.589	0.021201	190.65	189.39	0.660897

Table 14: Modeling parameters.

b	(mm)	Plate length
w	30 (mm)	Plate width
a	(mm)	Size of yielding area
r	(mm)	Cavity radius in plate center
H	1.5 (mm)	Plate thickness
E_1	50 (MPa)	Young's modulus in line with fibers
E_2	15.2 (MPa)	Young's modulus in the vertical direction in line with fibers
$E3$	15.2 (MPa)	Young's modulus out of plate
Nu12	0.254	Poisson's ratio
Nu13	0.254	Poisson's ratio
Nu23	0.428	Poisson's ratio
G12	4.7(MPa)	Shear modulus in 1 and 2 plates
G13	4.7(MPa)	Shear modulus in 1 and 3 plates
G23	3.28(MPa)	Shear modulus in 2 and 3 plates
$K_c = (N_{cr} * w)/(E_2 * h^3)$		Critical load of dimensionless tension

Table 15: Explained ratios for analysis and modeling.

Sizes of dimensionless sample	Size ratios in sample
a/r	0, 0/25, 0/5, 0/75, 1, 1/25, 1/5, 2, 2/5
r/w	0/1, 0/15, 0/2
b/w	1, 1/5, 2

4.1. Geometry Specifications of the Sample. The model has 30 mm width and length to width ratios are 1, 1.5, and 2, also the plate has a central cavity whose radius was designed in a ratio of 1% of the plate width, also these radii were generalized for 0/15 of plate width and 0/2 of plate width ratios. In modeling done, yielding dimensions were changed due to the size of central cavity (the central cavity was designed based on the drill head diameter in the drilling). Table 13 shows the different ratios used in this modeling. Due to the importance of boundary conditions in the tension treatments of plates, the four joint edge and two joint edge-two free edge were assessed in this research (Table 14). Since, the pressure loading is applied to two edges of the plate equally, and the object has geometry symmetry, assessment of available symmetry in the model is possible. In the researches done, with observance to the sustainability definitions and the symmetry conditions of samples, it has been modeled in the form of 1/4 (Table 15):

(1) Many elements existed in the complete modeling than 1/4 modeling.

(2) Frugality in the solution time and modeling also prevents available problems in the complete modeling.

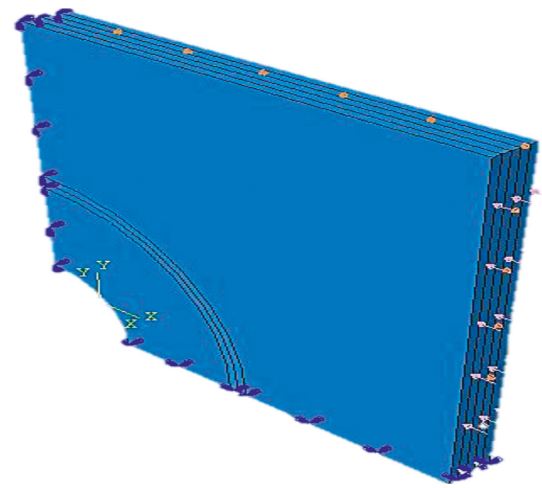

Figure 20: Plate under pressure loading.

4.2. Loading and Boundary Conditions. In this modeling, the main purpose is assessing the effects of plate dimensions, the cavity, and yielding on the value of critical tension load, so the loading is a kind of pressure loading which is applied to two edges parallel with y axis, since the model is designed as 1/4, just one outside edge of plate which is parallel with y axis has been applied under the pressure loading. The symmetrical boundary conditions are used for two internal edges of plate, the edge which is perpendicular to x axis and parallel to y axis, is limited in line with x. $U_1 = 0$ and its derivatives means $U_{R3} = 0$ and $U_{R2} = 0$ also were closed. For meshing of the modeling done, because of being three-dimensional and also available sensitivity, the crack modeling is used with high rank cubical elements with 20 knots, this element is known as C3D20R, in Abaqus software. Of

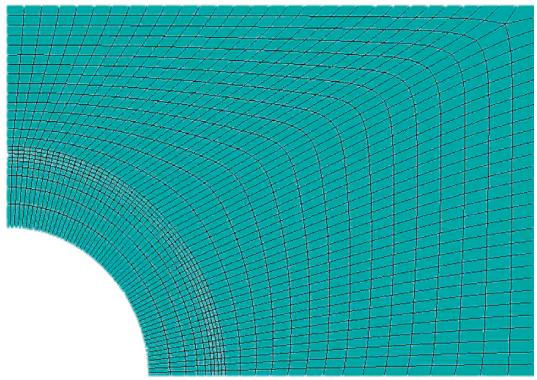

Figure 21: Plate meshing, front plate view of *x*-*y*.

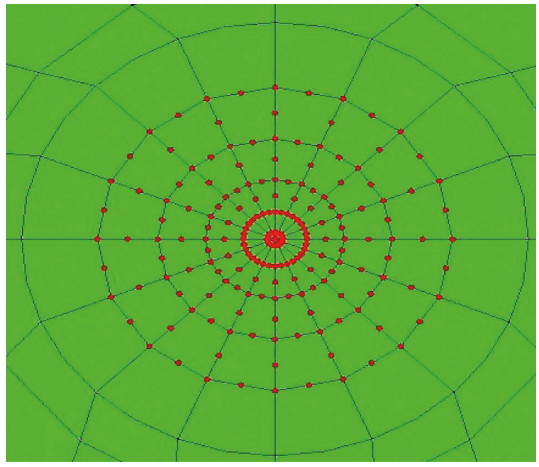

Figure 22: Meshing cantors around of crack tip.

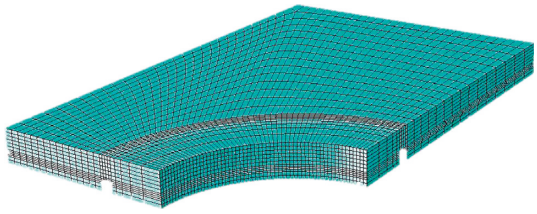

Figure 23: Over view of plate and shape of meshing done.

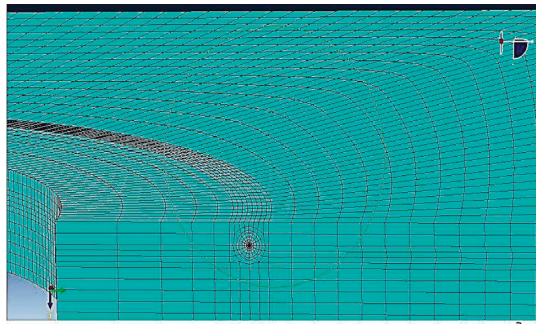

Figure 24: Location of yielding in plate.

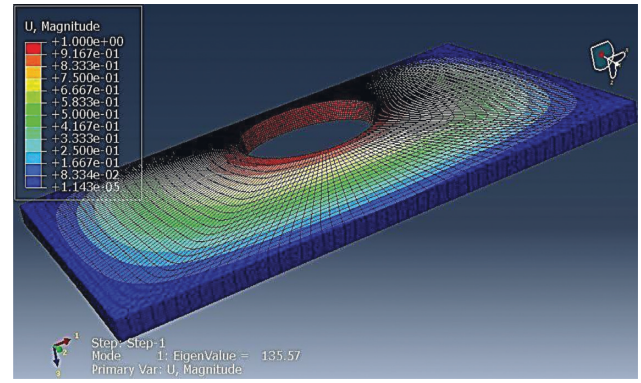

Figure 25: Tension mode for plate with 1/5 length to width ratio and 0/2 radius to width ratio without yielding.

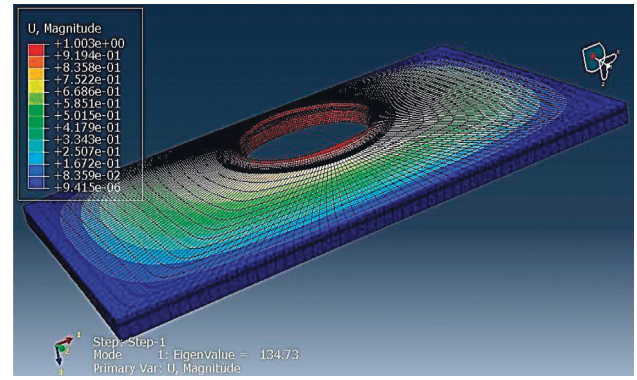

Figure 26: First tension mode for plate with 1/5 length to width ratio and 0/2 radius to width ratio with 0/25 yielding ratio.

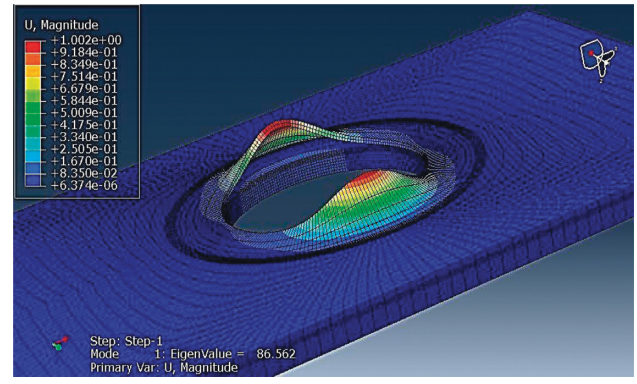

Figure 27: First tension mode for plate with 1/5 length to width ratio and 0/2 radius to width ratio with 0/5 yielding ratio.

course, available sensitivity in the tip of the crack, causes the elements be small enough in that area, and the wedge elements are used in the tip of the crack. Also based on the linear fatigue mechanics, the middle knots available in the tip of the crack were transferred to 1/4 of crack. In Figures 20–22, the singularity of the elements of the crack tip is showed, also based on the elastic linear fatigue mechanics, the middle transfer of the elements of the crack tip to 1/4 of their contour till crack tip is observable.

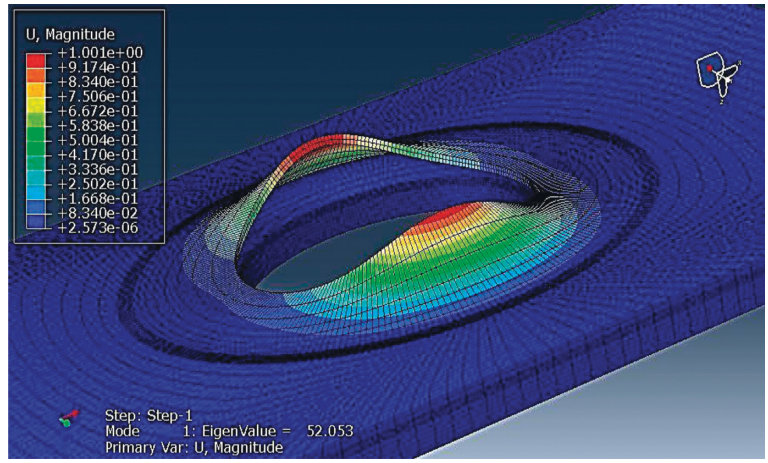

Figure 28: First tension mode for plate with 1/5 length to width ratio and 0/2 radius to width ratio with 0/75 yielding ratio.

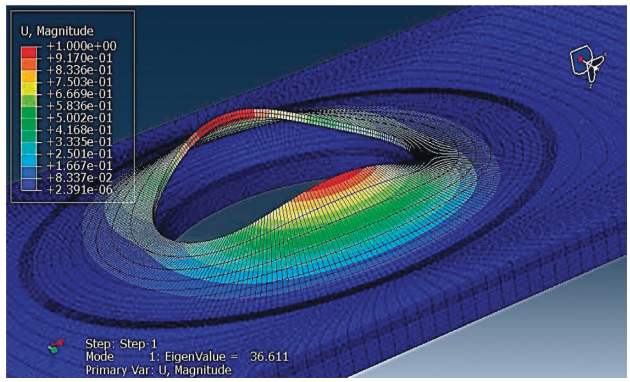

Figure 29: First tension mode for plate with 1/5 length to width ratio and 0/2 radius to width ratio with 1 yielding ratio.

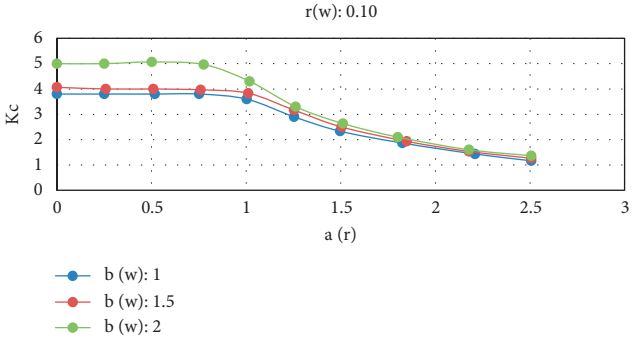

Figure 30: Dimensionless figure of tension coefficient according to crack length to radius ratios and different length to width for cavity with 0/1 ratio.

Figures 23 and 24 present the overview of the plate and also its meshing kind. One of the most important points in the three-dimensional models is the number of general and local granulation. Because the elements ring around the tip of the crack, and their growing up ratio, the number of seeds should be selected in the method which is creating the zero elements to be impossible (the zero elements are those ones in which their sides ratio has a lot of difference with each other). This matter is possible through the experience in meshing, using of different patterns for meshing, and correct granulation of elements ring around the crack line and the whole of the plate.

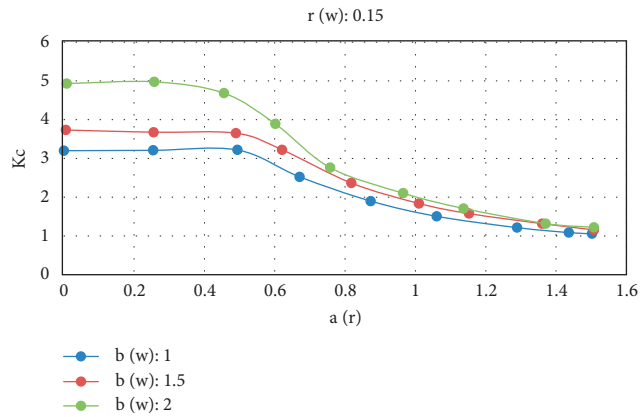

Figure 31: Dimensionless figure of tension coefficient according to crack length to radius ratios and different length to width for cavity with 0/15 ratio.

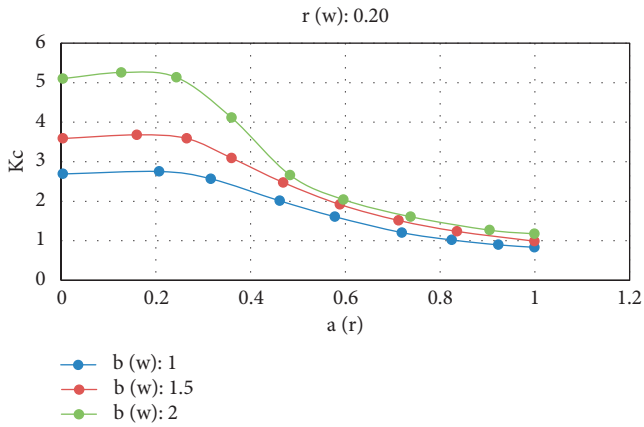

Figure 32: Dimensionless figure of tension coefficient according to crack length to radius ratios and different length to width for cavity with 0/2 ratio.

For example, critical modes of the tension for the plate with 1/5 length to width ratio and 0/2 radius to width ratio were assessed. As it is visible, by increasing the dimensions of yielding, the values of critical tension load decreased (Figures 25–29).

4.3. Analysis of Critical Tension Load Value for a Plate with Different Radii. In Figures 30 and 31, effects of the cavity dimensions on the critical tension load were assessed. As it is visible, for a specific radius without yielding, value of the critical tension load for the plate, gets bigger with length to width ratio. Also, by increasing the yielding area and converting the general tension to local tension, these values get convergent. Another visible point is increasing the difference of general tension values by increasing the cavity radius, in different length to width ratios of the plate. This matter shows the effect of cavity dimensions on the critical load of general tension in the plate, in Figure 32, the values of critical tension load for the plate including cavity with specific dimensions were expressed.

5. Conclusion

The figures showed that the plates with SSSS boundary conditions (joint-joint boundary conditions) have a higher value of critical tension load than that of SFSF boundary conditions (joint-free boundary conditions). While, in the joint-free boundary conditions, the critical tension load is decreased by increasing the length to width ratio, and in most cases, the tensions are a kind of general. Therefore, through the assessment and detailed analysis of tension, the permissible tension of desired cross section can be determined, until we do not exceed from the limit which this is the main step in designing of the machinery and the desired structures. On the other hand, by knowing the permissible tension and specific cross section, the maximum loading can be calculated, and this is the quality control. By increasing the dimensions of yielding, value of the critical tension load is decreased, and the kind of the tension from general tension is changed to local tension. In the joint-free boundary conditions, because of plate tension treatment, the effects of the yielding are decreased, and in most cases, the tension is a kind of general one. Increase in diameter of central cavity causes the decrease in the value of critical tension load, of course, by increasing the length to width ratio in the plate, effects of the central cavity will be decreased. Effect of edge crack on critical tension load in perforated plate: the yielding dimensions is one of the most important properties in the research done, yielding is an important factor in the value of critical tension load in the plate, in addition to the effective role on the critical tension load, this parameter determines the kind of tension (general or local). By increasing the dimensions of yielding, the value of critical tension load is decreased. However, by growing the yielding dimensions, the general tension is changed to local tension and values of the local critical tension load in these two boundary conditions will be convergent to each other. For $b/w = 1$, $b/w = 1/5$, and $b/w = 2$, the rate of decline in values of local critical tension load is, respectively, 0/89%, 16/98%, and 51/68%.

Kind of the boundary conditions has effect on the value of the critical tension load and the kind of tension created, in the joint-joint boundary conditions, the critical tension load is increased by increasing the length to width ratio, and the local tension occurred in higher yielding ratio. This is because of the tension treatment of the plate with SFSF boundary conditions and its similarity with tension of the columns. Surrounded kind of tension in the SFSF boundary conditions is general tension. In the event that the SSSS boundary conditions causes increase in the critical tension load, and also in bigger dimensions creates the yielding, the local tension will be the main reason of tension in the SSSS boundary conditions. Due to the figures, for the mode which $b/w = 1$, the values of general critical tension load in the SFSF boundary conditions are decreased to 40% of the SSSS boundary conditions. Also, for $b/w = 1/5$ and $b/w = 2$, the rate of decline of general critical tension load is, respectively, 72/8 and 87/7. Effect of plate dimensions (length to width ratio) on critical tension load of perforated plate including yielding: one of other effective and important parameters on the critical tension load is length to width ratio of the plate, in the SSSS boundary conditions, by increasing the length to width ratio, value of the critical tension load is increased, which, by increasing the length, has joint boundary conditions in the direction of the load. But treatment of the critical tension load for SFSF boundary conditions is different, by increasing the length to width ratio, the critical tension load is decreased. Also, for the length to width ratios more than 1, in most cases, the tension is a kind of general tension. Also, due to the cavity dimensions and boundary conditions, range of the tension kind changes from general tension kind to local tension kind. Effect of central cavity dimensions on critical tension load in perforated plate including yielding: the size of central cavity radius is one of effective factors on the critical tension load. By increasing it, in SSSS and SFSF boundary conditions, the value of the critical tension load is decreased, but the rate of decrease, in critical tension load, has downward trend by increasing the length to width ratio (effect of the cavity radius on the critical tension load will be decreased by increasing the length).

Data Availability

The data are available from the corresponding author upon request (mojtabanazari_1350@yahoo.com).

Conflicts of Interest

The authors declare that there are no conflicts of interest regarding the publication of this paper.

References

[1] M. F. Haider, M. Y. Bhuiyan, B. Poddar, B. Lin, and V. Giurgiutiu, "Analytical and experimental investigation of the interaction of Lamb waves in a stiffened aluminum plate with a horizontal crack at the root of the stiffener," *Journal of Sound and Vibration*, vol. 431, pp. 212–225, 2018.

[2] T. Hao and Z. M. Hossain, "Atomistic mechanisms of crack nucleation and propagation in amorphous silica," *Physical Review B*, vol. 100, no. 1, Article ID 014204, 2019.

[3] S. Abedini, C. Dong, and I. J. Davies, "Finite element analysis of edge crack delamination and optimisation of functionally graded interlayer for coated stainless steel in hydrogen storage applications," *Surface and Coatings Technology*, vol. 372, pp. 148–159, 2019.

[4] M. Jafari, "Thermal stress analysis of orthotropic plate containing a rectangular hole using complex variable method," *European Journal of Mechanics - A: Solids*, vol. 73, pp. 212–223, 2019.

[5] F. Barras, M. Aldam, T. Roch, E. A. Brener, E. Bouchbinder, and J. F. Molinari, "The emergence of crack-like behavior of frictional rupture: edge singularity and energy balance," *Earth and Planetary Science Letters*, vol. 531, Article ID 115978, 2020.

[6] R. Seifi, "Total fatigue lives, crack growth paths and cycles in cold expanded adjacent holes," *International Journal of Fatigue*, vol. 113, pp. 69–77, 2018.

[7] R. Rihan, B. Al-Wakaa, N. Tanoli, and H. Shalaby, "The susceptibility of P110 downhole tubular steel to sulfide stress cracking in H2S and NaCl," *Journal of Petroleum Science and Engineering*, vol. 174, pp. 1034–1041, 2019.

[8] A. E. Seif and M. Z. Kabir, "Experimental study on the fracture capacity and fatigue life reduction of the tensioned cracked plate due to the local buckling," *Engineering Fracture Mechanics*, vol. 175, pp. 168–183, 2017.

[9] S. M. Nahid, S. Nahian, M. Motalab, T. Rakib, S. Mojumder, and M. M. Islam, "Tuning the mechanical properties of silicene nanosheet by auxiliary cracks: a molecular dynamics study," *RSC Advances*, vol. 8, no. 53, pp. 30354–30365, 2018.

[10] H. Niazi, G. Nelson, L. Lamborn, R. Eadie, W. Chen, and H. Zhang, "Crack Growth Sensitivity to the Magnitude and Frequency of Load Fluctuation in Stage 1b of High pH Stress Corrosion Cracking," *Corrosion*, vol. 77, p. 3711, 2021.

[11] B. J. Wang, D. K. Xu, J. Sun, and E. H. Han, "Effect of grain structure on the stress corrosion cracking (SCC) behavior of an as-extruded Mg-Zn-Zr alloy," *Corrosion Science*, vol. 157, pp. 347–356, 2019.

[12] Y. Zhao, Y. Wang, W. Wang, L. Tang, Q. Liu, and G. Cheng, "Modeling of rheological fracture behavior of rock cracks subjected to hydraulic pressure and far field stresses," *Theoretical and Applied Fracture Mechanics*, vol. 101, pp. 59–66, 2019.

[13] H. Tian, X. Wang, Z. Cui et al., "Electrochemical corrosion, hydrogen permeation and stress corrosion cracking behavior of E690 steel in thiosulfate-containing artificial seawater," *Corrosion Science*, vol. 144, pp. 145–162, 2018.

[14] E. Alizadeh and M. Dehestani, "Analytical and numerical fracture analysis of pressure vessel containing wall crack and reinforcement with CFRP laminates," *Thin-Walled Structures*, vol. 127, pp. 210–220, 2018.

[15] M. Hamrat, F. Bouziadi, B. Boulekbache et al., "Experimental and numerical investigation on the deflection behavior of precracked and repaired reinforced concrete beams with fiber-reinforced polymer," *Construction and Building Materials*, vol. 249, Article ID 118745, 2020.

[16] E. Martínez-Pañeda, V. S. Deshpande, C. F. Niordson, and N. A. Fleck, "The role of plastic strain gradients in the crack growth resistance of metals," *Journal of the Mechanics and Physics of Solids*, vol. 126, pp. 136–150, 2019.

[17] M. Heydari-Meybodi, M. R. Ayatollahi, and F. Berto, "Rupture analysis of rubber in the presence of a sharp V-shape notch under pure mode-I loading," *International Journal of Mechanical Sciences*, vol. 146-147, pp. 405–415, 2018.

[18] J. Torabi and R. Ansari, "Numerical phase-field vibration analysis of cracked functionally graded GPL-RC plates," *Mechanics Based Design of Structures and Machines*, vol. 1, pp. 1–20, 2020.

[19] M. Heydari-Meybodi, M. R. Ayatollahi, and F. Berto, "Averaged strain energy density criterion for rupture assessment of cracked rubbers: a novel method for determination of critical SED," *Engineering Fracture Mechanics*, vol. 190, pp. 93–103, 2018.

[20] T. Du, M. Blum, C. Chen, M. G. Muraleedharan, A. C. van Duin, and P. Newell, "Nanomechanical investigation of the interplay between pore morphology and crack orientation of amorphous silica," *Engineering Fracture Mechanics*, vol. 250, Article ID 107749, 2021.

[21] T. Ahmed, A. Yavuz, and H. S. Turkmen, "Fatigue crack growth simulation of interacting multiple cracks in perforated plates with multiple holes using boundary cracklet method," *Fatigue and Fracture of Engineering Materials and Structures*, vol. 44, no. 2, pp. 333–348, 2021.

[22] N. Hasebe, K. Tamai, and T. Nakamura, "Analysis of kinked crack under uniform heat flow," *Journal of Engineering Mechanics*, vol. 112, no. 1, pp. 31–42, 1986.

[23] S. A. Aseeri, "Goursat functions for a problem of an isotropic plate with a curvilinear hole," *Int. J. Open Problems Compt. Math*, vol. 1, no. 3, 2008.

[24] P. C. Vinh, N. Hasebe, X. F. Wang, and T. Saito, "Interaction between a cracked hole and a line crack under uniform heat flux," *International Journal of Fracture*, vol. 131, no. 4, pp. 367–384, 2005.

[25] C. F. Gao, Y. T. Zhao, and M. Z. Wang, "An exact and explicit treatment of an elliptic hole problem in thermopiezoelectric media," *International Journal of Solids and Structures*, vol. 39, no. 9, pp. 2665–2685, 2002.

[26] Y. Xu, D. Zhou, and K. Liu, "Three-dimensional thermoelastic analysis of rectangular plates with variable thickness subjected to thermomechanical loads," *Journal of Thermal Stresses*, vol. 33, no. 12, pp. 1136–1155, 2010.

[27] N. Sarkar and A. Lahiri, "A three-dimensional thermoelastic problem for a half-space without energy dissipation," *International Journal of Engineering Science*, vol. 51, pp. 310–325, 2012.

[28] P. F. Hou, H. Y. Jiang, and Q. H. Li, "Three-dimensional steady-state general solution for isotropic thermoelastic materials with applications I: general solutions," *Journal of Thermal Stresses*, vol. 36, no. 7, pp. 727–747, 2013.

[29] M. Fal, R. Hussein, K. Chandrashekhara, A. Abutunis, and V. Menta, "Experimental and numerical failure analysis of horizontal axis water turbine carbon fiber-reinforced composite blade," *Journal of Renewable and Sustainable Energy*, vol. 13, no. 1, Article ID 014501, 2021.

[30] H. Ardebili, M. Amin, J. W. Salamon, and S. Mahdi Seyed-Kolbadi, "Discussion of "hydrodynamic pressure on gravity dams with different heights and the westergaard correction formula" by mingming wang, jianyun chen, liang Wu, and

bingyue song," *International Journal of Geomechanics*, vol. 22, no. 8, Article ID 07022006, 2022.

[31] A. Solomon and T. Alemu Mohammed, "Structures under synergetic effects of combined blast and impact loads: a state-of-the-art review," *Advances in Civil Engineering*, vol. 2022, Article ID 6934078, 30 pages, 2022.

[32] S. Shen, Y. Zhao, L. Chang, S. Dai, F. Wu, and M. Jiang, "Penetration form of inter-hole cracks under double-hole blasting conditions with inclined fissures," *Advances in Civil Engineering*, vol. 2021, Article ID 6677595, 13 pages, 2021.

[33] S. M. Seyed Kolbadi, N. Hassani, S. M. Seyed-Kolbadi, and M. Mirtaheri, "Analyzing parametric sensitivity on the cyclic behavior of steel shear walls," *Shock and Vibration*, vol. 2021, 2021.

[34] K. Gao, G. Qiao, Z. Liu, and W. Xia, "Damage characteristics caused by deep-hole blasting near normal fault and its effects on coal and gas outbursts," *Geofluids*, vol. 2022, Article ID 2421492, 13 pages, 2022.

[35] M. Mirtaheri, M. Salkhordeh, S. M. Kolbadi, H. Mirzaeefard, and M. R. Razzaghian, "Evaluation of 2D concentrically braced frames with cylindrical dampers subjected to near-field earthquake ground motions," *Numerical Methods in Civil Engineering*, vol. 4, no. 3, pp. 21–30, 2020.